

# Development of an artificial neural network model for estimating the radius ratio of a one-layered cylindrical shell

Y. Khandouch<sup>a,\*</sup>, El H. Aassif<sup>a</sup>, S. Agounad<sup>a</sup>, G. Maze<sup>b</sup>

<sup>a</sup>Laboratory of Metrology and Information Processing, Faculty of Science, Ibn Zohr University, B.P 8106 Agadir, Morocco

<sup>b</sup>Laboratory of Waves and Complex Areas FRE CNRS, Havre University, Place Robert Schuman, 76610 Le Havre, France

Received 1 March 2019; accepted 17 December 2020

---

## Abstract

The results obtained from previous studies on the acoustic scattering of a plane wave by an elastic cylindrical shell, show that the acoustic resonances of the shell are related to its physical and geometrical properties. In order to estimate the radius ratio of an air-field immersed cylindrical shell, an approach based on artificial neural networks was proposed, which uses the reduced cutoff frequencies of circumferential waves that propagate around the cylindrical shell. The reduced cutoff frequencies of circumferential waves are extracted using modal isolation plan representation. The proposed approach allows us to estimate accurately the values of the radius ratio of the copper cylindrical shell, as well as it can help us to resolve other problems related to acoustic scattering. Furthermore, it can be used to estimate other parameters of the cylindrical shell starting from the characteristics of which it is disposed. The approach proposed in this study does not present any approximation as in the case of the proper mode theory.

© 2020 University of West Bohemia. All rights reserved.

**Keywords:** cylindrical shell, radius ratio, circumferential waves, reduced cutoff frequencies, modal isolation plan, artificial neural networks

---

## 1. Introduction

If an air-filled elastic cylindrical shell with inner-to-outer radius ratio  $b/a$  is immersed in water and excited by a plane acoustic wave perpendicularly to its axis, circumferential waves are generated automatically in the shell and in the water-shell interface. Two types of circumferential waves are observed: antisymmetric waves  $A_i$  and symmetric waves  $S_i$  [25, 26]. For some frequencies, these circumferential waves create standing waves on the circumference of the cylindrical shell constituting resonances. These resonances are noticed on the spectrum of the form function [8, 13]. The previous theoretical works [22, 27], and experimental studies [14, 23] or [28] show that the acoustic resonances are linked to the geometrical and physical properties of the shell. Inversely, starting from the resonances of circumferential waves, we can characterize the geometry of the cylindrical shell and the material that it is made of. Some of these studies use an approximate approach which is based on the assimilation of the cylindrical shell to a plate with the same thickness [19]. As in the case of the proper mode theory, which uses the resemblance between circumferential waves propagate in the case of cylindrical shell, and Lamb waves propagates in the case of a plat. This similarity is relevant to a thin cylindrical shell that has the radius ratio  $b/a \geq 0.90$ . It enables the use of the traditional relationships established in the case of Lamb waves in order to get the value of the reduced cutoff frequencies

---

\*Corresponding author. Tel.: +212 622 529 105, e-mail: khandouch.younes@edu.uiz.ac.ma.  
<https://doi.org/10.24132/acm.2020.533>

of circumferential waves propagate around the cylindrical shell. In our recent study [17], the soft computing techniques are used to build a model in order to estimate the radius ratio of the cylindrical shell directly from its form function. The analyses carried out on the findings show that the proposed model presents some limitation and must be improved.

In this work, in order to estimate the radius ratio  $b/a$  of the elastic cylindrical shell, we examined the use of the reduced cutoff frequencies of circumferential waves. These frequencies can be identified from the resonance spectrum, the time-frequency image [3], or from the modal isolation plan representation of the form function [21, 23]. In this paper, a comparative study was done in order to examine the quality and difficulties in estimating the reduced cutoff frequency values, especially for thick cylindrical shells ( $b/a < 0.90$ ). The studied cylinders are made from copper with radius ratio varying from 0.50 to 0.99. The estimated reduced cutoff frequencies are implemented in a model based on the artificial neural networks technique [30]. Lately, the artificial neural networks have been used to resolve some problems related to the acoustic scattering, as noticed in [1, 10, 17] or [18]. During model development, the artificial neural networks are trained by Levenberg-Marquardt back-propagation algorithm to obtain a high generalization accuracy [16]. To build a reliable and robust neural network architecture, the  $k$ -fold cross-validation strategy was used [6, 29]. In summary, the proposed method enables to estimate the values of radius ratio of copper cylinders with good precision. The proposed model can be generalized to other waves not used in this study, and can be applied to other cylindrical shells made from different materials.

## 2. Acoustic scattering from an elastic cylindrical shell

If an air-filled elastic cylindrical shell made from a given material with radius ratio  $b/a$  ( $a$ : outer radius,  $b$ : inner radius) is immersed in water and excited by a plane acoustic wave, the resonances are noticed on the spectrum of the scattering acoustic pressure by the shell. Fig. 1 indicates the cylindrical shell, the coordinate orientation, the direction of the incident plane wave, and the scattered acoustic pressure; which is the summation of the waves that take into account the effects of the incident wave, the reflective wave {1}, the circumferential waves in the shell {2} (whispering gallery wave, Rayleigh wave), and the interface Scholte wave {3} connected to the geometry of the object. This was stated in different works [7, 13, 15, 21, 24] and [28].

The incident acoustic pressure  $P_{\text{inc}}(\omega, \theta, r)$  can be expressed as follows:

$$P_{\text{inc}}(\omega, \theta, r) = P_0 \sum_{n=0}^{+\infty} j^n \varepsilon_n J_n(K_1 r) \cos(n\theta) \exp(-j\omega t), \quad (1)$$

where  $P_0$  is the amplitude of the incident plane wave,  $J_n(K_1 r)$  is the Bessel function of the first kind and order  $n$ ,  $k_1 = \omega/C_1$  is the wave number, where  $\omega$  is the angular frequency and  $C_1$  is the wave velocity in the external fluid,  $\varepsilon_n$  is the Neumann coefficient ( $\varepsilon_n = 1$  if  $n = 0$  and  $\varepsilon_n = 2$  if  $n \neq 0$ ),  $j^2 = -1$ ,  $\theta$  is the azimuthal angle, and  $r$  is the distance between the revolution axis of the cylindrical shell and the position where the scattering acoustic pressure is calculated.

The scattered acoustic pressure  $P_{\text{scat}}(\omega, \theta, r)$  can be expressed as

$$P_{\text{scat}}(\omega, \theta, r) = P_0 \sum_{n=0}^{+\infty} j^n b_n H_n^1(K_1 r) \cos(n\theta) \exp(-j\omega t), \quad (2)$$

where  $b_n = D_n^1(\omega)/D_n(\omega)$  is the coefficient that describes the acoustic scattering in water,  $D_n^1(\omega)$  and  $D_n(\omega)$  are determinants computed from the boundary conditions of the problem [23], and  $H_n^1(K_1 r)$  is the Hankel function of the first kind of order  $n$ .

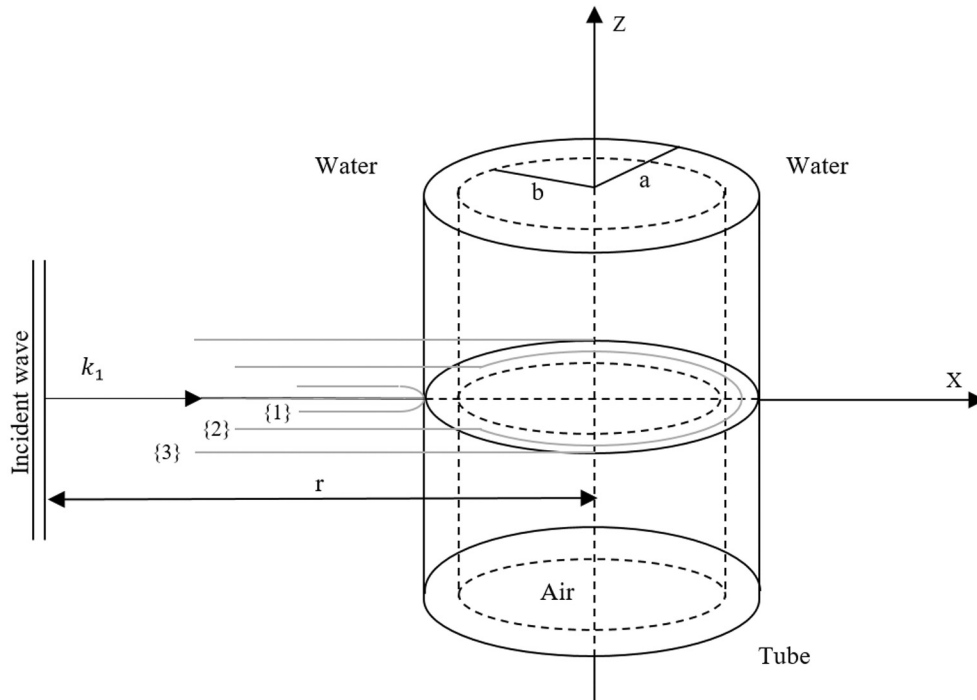


Fig. 1. Mechanisms of the formation of the scattering acoustic pressure

To describe the acoustic scattering from a cylindrical shell, we use the form function which can be expressed in a far field by

$$F_{\infty}(x_1, \theta) = |f_{\infty}(x_1, \theta)| \approx \lim_{r \rightarrow +\infty} \sqrt{\frac{2r}{a}} \left| \frac{p_{\text{scat}}}{p_{\text{inc}}} \right|, \quad (3)$$

$$F_{\infty}(x_1, \theta) = \left| \sum_{n=0}^{+\infty} f_n(x_1, \theta) \right|, \quad (4)$$

where

$$F_{\infty}(x_1, \theta) = \frac{2}{\sqrt{\pi x_1}} \left| \sum_{n=0}^{+\infty} \varepsilon_n b_n \cos(n\theta) \right|, \quad (5)$$

where  $x_1 = ka$  is the reduced frequency written as follows:

$$x_1 = ka = \frac{2\pi\nu a}{C_1}, \quad (6)$$

where  $\nu$  is the wave frequency in hertz.

To compute the form function in a far field as a function of the reduced frequency  $ka$ , we considered the backscattering field ( $\theta = \pi$ ). The physical parameters used in this work are given in Table 1.

Table 1. Physical parameters

	Density $\varrho$ [kg/m <sup>3</sup> ]	Longitudinal velocity $C_l$ [m/s]	Transverse velocity $C_t$ [m/s]
Copper	8 920	4 760	2 325
Water	1 000	1 470	–
Air	1.29	324	–

### 3. Estimation of circumferential wave reduced cutoff frequencies

The circumferential waves propagate around the cylindrical shell are characterized by the reduced cutoff frequencies, which can be estimated from the resonance spectrum, the time-frequency image, or from the modal isolation plan of the form function. These techniques have been applied to solve several problems related to the acoustic scattering [4, 5] or [11]. Many works are limited to thin cylindrical shells. In this current research, to present the confronted problems, we have chosen two examples of cylindrical shells: a thin cylindrical shell ( $b/a = 0.93$ ) and a thick cylindrical shell ( $b/a = 0.70$ ). Figs. 2 and 3 show the form function of the considered cylindrical shells. These figures show that the acoustic pressure is composed of two parts, resonant and non-resonant. The resonant part strongly oscillates and is related to the resonances of the circumferential waves. The non-resonant part is referred to the reflective wave at the outer interface of the cylindrical shell, median values around 1. From these figures, we can notice that with increasing thickness of the cylindrical shell, the radius ratio decreases; more crowded scene is noticed as well, as the increase in the generated circumferential waves. Therefore, the observed interval is reduced for the thick cylindrical shell to keep the same number of observed waves.

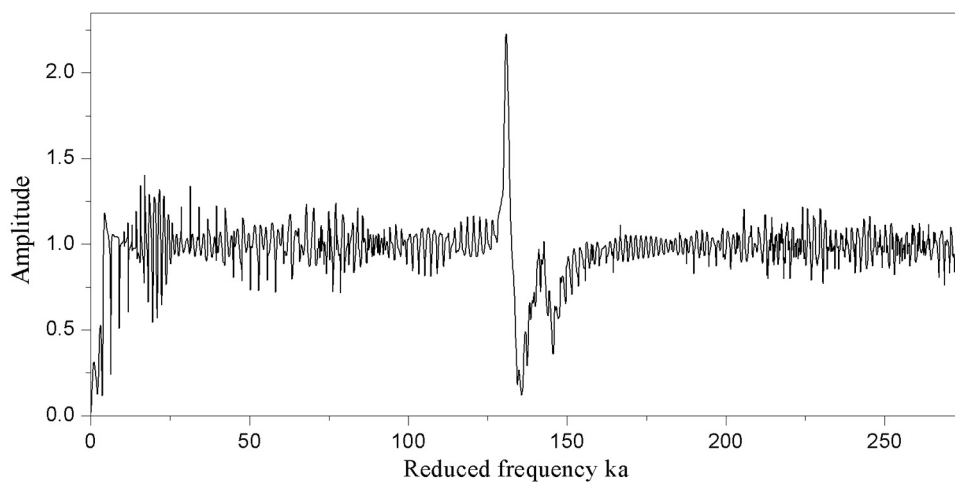


Fig. 2. Form function of the thin copper cylindrical shell ( $b/a = 0.93$ )

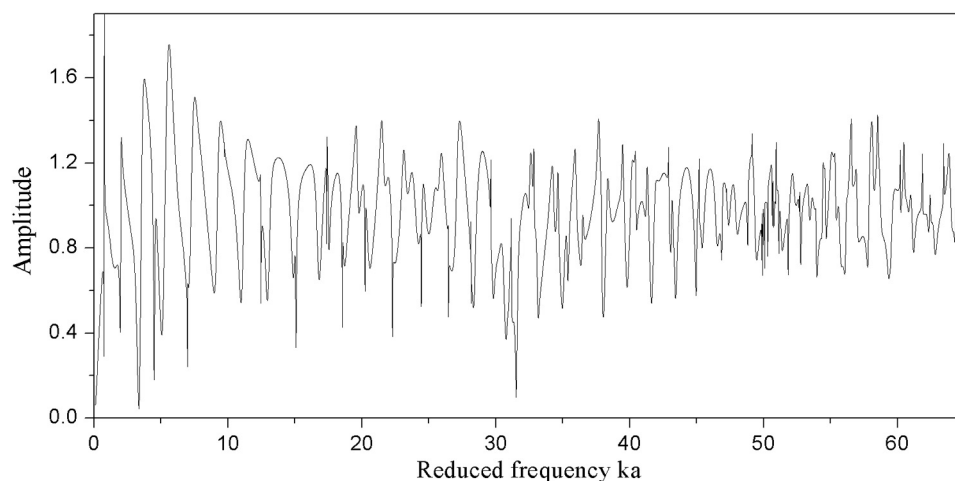


Fig. 3. Form function of the thick copper cylindrical shell ( $b/a = 0.70$ )

### 3.1. Methods

#### 3.1.1. Resonance spectrum

To obtain the resonance spectrum, the inverse Fourier transform is firstly applied to the from function to get the time impulse response

$$P_{\text{scatt}}(t) = \frac{1}{2\pi} \int_{-\infty}^{+\infty} h(ka) F_{\infty}(ka, \theta) \exp(j\omega t) d\omega, \quad (7)$$

where  $h(ka)$  represents the bandpass of the transducer used in the experiments [13,24].

After that, the specular echo is replaced by zeros at the beginning of the time impulse response which is related to the reflection on the outer surface of the cylindrical shell. Finally, to obtain the resonance spectrum, the direct Fourier transform is applied on the new time impulse response [23].

#### 3.1.2. Time-frequency image

The Smoothed Pseudo Wigner-Ville (SPWV) distribution was applied to the time impulse response in which the specular echo was replaced by zeros to obtain the time-frequency image. The time-frequency representation takes into account both time and frequency parameters [12], leading to an image that allows to follow the evolution of the frequency as a function of time. It becomes straightforward to identify the different frequency components. In the present research, the SPWV distribution is used for its interesting properties [9, 20], since it provides a representation well localized in time and frequency. The SPWV distribution is a variant of the Wigner-Ville distribution. It has been proposed to reduce the interference terms appearing between the components of the studied signal in the time-frequency plane of the WV distribution. The SPWV distribution can be written as

$$SPWV_{g,h}(t, \nu) = \int \int h(\tau) g(u - \tau) x_a(u + \frac{\tau}{2}) x_a^*(u - \frac{\tau}{2}) \exp(-j2\pi\nu\tau) du d\tau, \quad (8)$$

where  $h$  and  $g$  are two real even windows corresponding to time and frequency smoothing, and  $x_a(t)$  is the analytical signal of  $x(t)$  which is written as follows  $x_a(t) = x(t) + j\hat{x}(t)$ , where  $\hat{x}(t)$  is the Hilbert transform of  $x(t)$  expressed by

$$\hat{x}(t) = \frac{1}{\pi} \int_{-\infty}^{+\infty} \frac{x(\tau)}{t - \tau} d\tau. \quad (9)$$

#### 3.1.3. Modal isolation plan

When the circumferential wave is generated on the shell, the resonances appear when the number of wavelengths on the circumference of the cylindrical shell is an integer. This integer is the mode  $n$  [13]. The form function is the summation of the modes of vibration  $n$  for each frequency. By separating the contribution of each mode  $n$ , we got the partial form function associated with each mode. The resonance spectrum assesses the frequency of observable resonances. The modal isolation plan is an alternative representation to this spectrum [21]. Each horizontal line of the plan is linked to a single mode obtained from the partial form function  $f_{\infty}^n$  [23]. This plan is the result of the following four steps:

**Step 1.** Compute the partial form function  $f_{\infty}^n$  ( $F_{\infty} = \sum_{n=0}^{n_{\text{max}}} f_{\infty}^n$ ) which is linked to mode  $n$  on the form function  $F_{\infty}$ .

**Step 2.** Apply the inverse Fourier transform to the partial form function  $f_{\infty}^n$  to obtain the partial impulse response.

**Step 3.** Replace the specular echo with zeros at the beginning of the partial impulse response.

**Step 4.** Compute the partial resonance spectrum by applying the direct Fourier transform to the new partial impulse response.

These steps are applied for each mode  $n$ . Finally, all partial resonance spectrums are assembled to obtain the modal isolation plan.

### 3.2. Application

Figs. 4 and 5 present the impulse response without specular echo, the resonance spectrum, and the time-frequency image for copper cylindrical shells with  $b/a = 0.93$  and  $b/a = 0.70$ , respectively.

The time impulse response in which we replaced the specular echo with zeros for the considered cylindrical shells is presented in Figs. 4(b) and 5(b). In this time impulse response, we can distinguish two parts: first, the non-resonant part known as specular echo, characterized

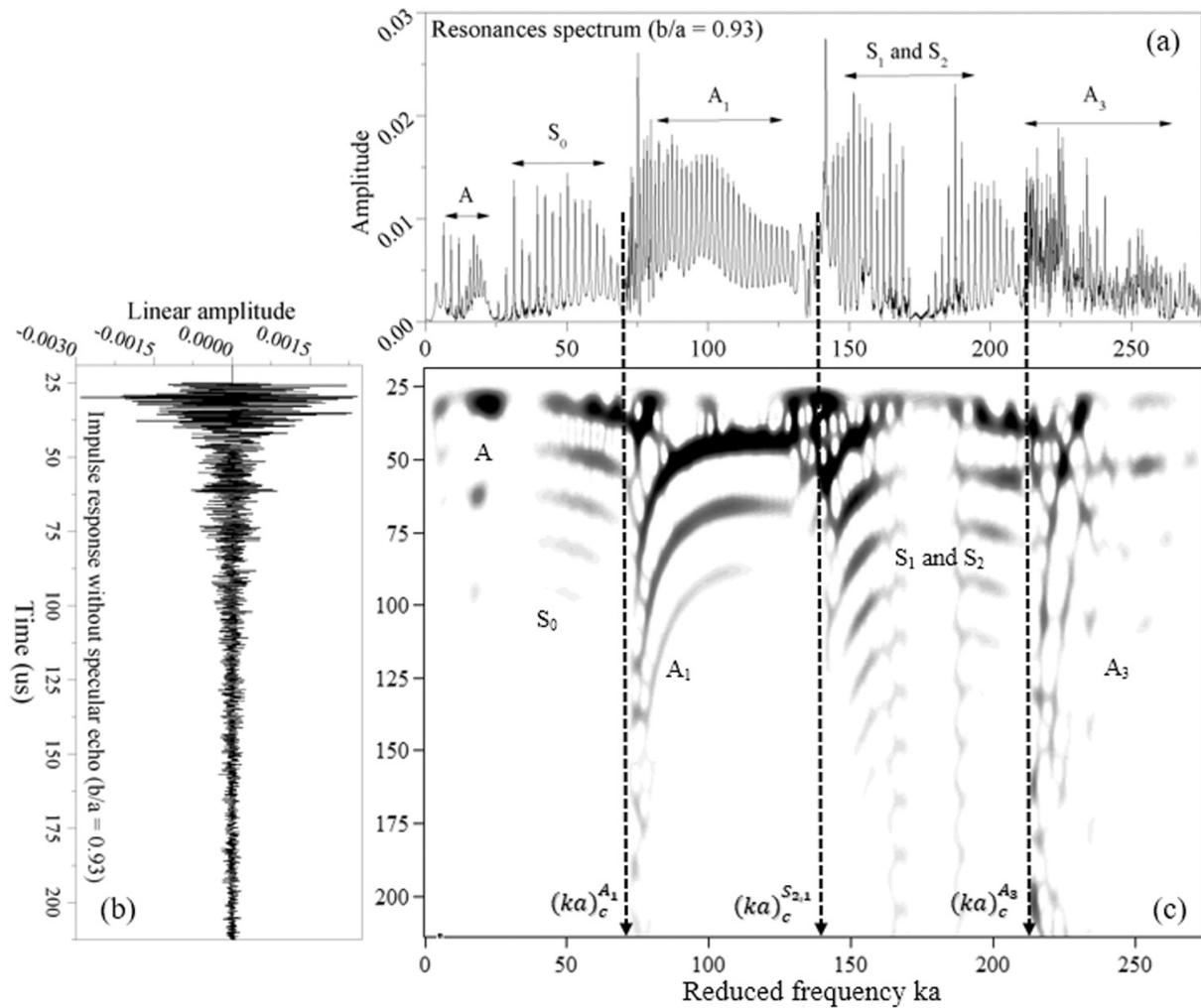


Fig. 4. (a) Resonance spectrum, (b) impulse response on which the specular echo is replaced by zeros, and (c) time-frequency image of the copper cylindrical shell with radius ratio  $b/a = 0.93$ . The vertical arrows refer to the reduced cut-off frequency of the  $A_1$ ,  $A_3$ ,  $S_1$  and  $S_2$  waves

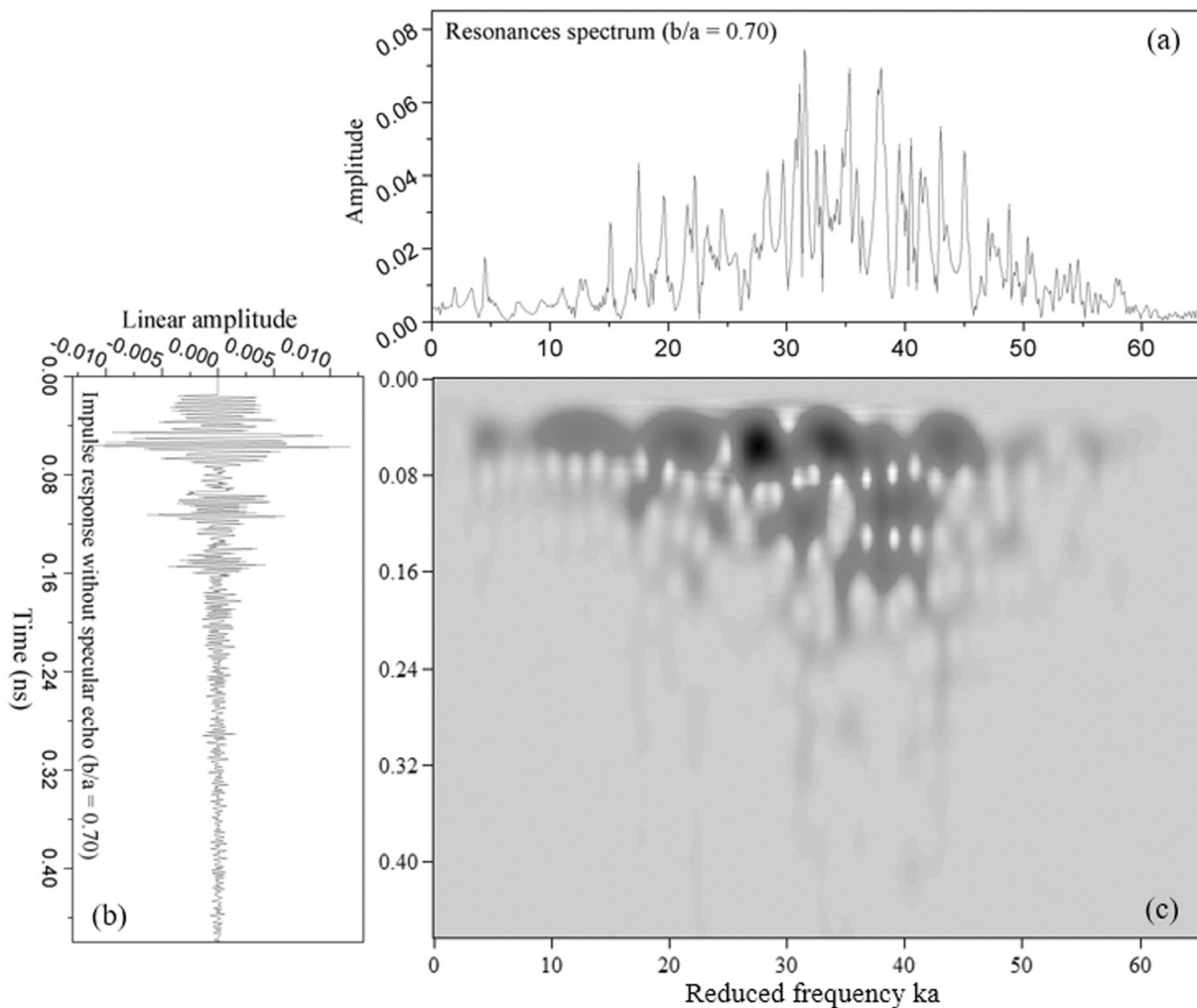


Fig. 5. (a) Resonance spectrum, (b) impulse response on which the specular echo is replaced by zeros, and (c) time-frequency image of the copper cylindrical shell with radius ratio  $b/a = 0.70$

by a large amplitude, brief duration and localized at the beginning of this impulse response. The second one is the resonant part characterized by a small amplitude, which is the succession of echoes related to the circumferential waves. One of the main advantages of this treatment is the possibility to suppress the specular echo. Figs. 4(a) and 5(a) show the resonance spectrum for the considered structures. The resonance spectrum is full of peaks and dips which indicate the resonance frequencies of the studied cylindrical shells. These frequencies are very interesting for material and geometrical characterization purpose. In Fig. 4(a), we have indicated the frequencies related to the different circumferential waves. The obtained time-frequency images by applying the SPWV distribution of the time impulse response of the considered cylindrical shells are presented in Figs. 4(c) and 5(c). On the one hand, the time-frequency analysis gives us the opportunity to analyze the frequency content of the circumferential waves as a function of time, and on the other hand, it enables us to determine their reduced cutoff frequencies [2]. Moreover, the time-frequency image is practical to identify the appearance time of circumferential waves echoes, which are difficult to identify from the time-analysis due to the overlapping phenomenon. This observation is related to the thin cylindrical shell in Fig. 4(b), and for the thick cylindrical shell, the obtained image is presented in Fig. 5(b).

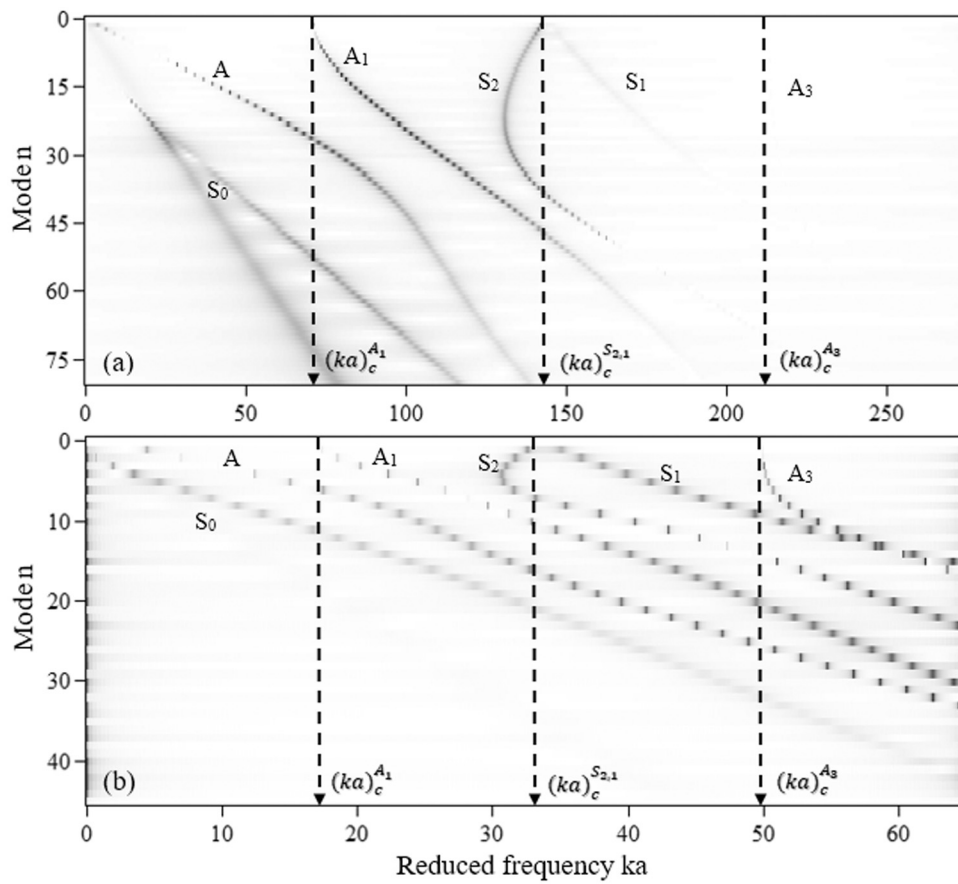


Fig. 6. Resonance trajectories of the copper cylindrical shells: (a)  $b/a = 0.93$  and (b)  $b/a = 0.70$

Table 2. Reduced cutoff frequencies of  $S_1$ ,  $S_2$ ,  $A_1$  and  $A_3$  waves of the copper cylindrical shells with  $b/a = 0.93$  and  $b/a = 0.70$

	$b/a = 0.93$			$b/a = 0.70$		
	$A_1$	$S_2, S_1$	$A_3$	$A_1$	$S_2, S_1$	$A_3$
Resonance spectrum	71.6	143.06	211.0	–	–	–
Time-frequency image	71.9	140.90	212.3	–	–	–
Modal isolation plan	71.2	141.80	213.2	17.3	32.5	49.8

To recognize the different ranges observed in the resonance spectrum, especially for the thick cylindrical shell, the modal isolation plan representation is applied. For the study of cylindrical shells, the obtained resonance trajectories are presented in Fig. 6. Each trajectory is linked with the corresponding wave. From this plan, we can identify the reduced cutoff frequencies of circumferential waves which are given by the intersection of frequency axis and the vertical asymptote of the wave trajectory for the smallest value of  $n$ . Vertical arrows on Figs. 4–6 refer to the reduced cutoff frequencies of circumferential waves ( $S_1$ ,  $S_2$ ,  $A_1$  and  $A_3$ ). As a result of applying those analysis methods, the obtained frequencies are presented in Table 2.

In summary, the findings show that the resonance spectrum and the time-frequency image can be used to estimate the reduced cutoff frequencies of circumferential waves for thin cylindrical

shells ( $b/a \geq 0.90$ ). However, for thick cylindrical shells ( $b/a < 0.90$ ), these representations become limited. The modal isolation plan in Fig. 6 shows a fineness and clearness of resonance trajectories for both thin and thick cylindrical shells. This method allows us to estimate the reduced cutoff frequency easily and accurately. For a given wave, the reduced cutoff frequency is determined for the small values of mode  $n$ . For the smallest value of  $n$ , Fig. 6 shows that the waves  $S_1$  and  $S_2$  are very close to each other. This means that their reduced cutoff frequencies are very close. In the rest of this study, the same value of the reduced cutoff frequencies will be taken for both waves. As shown in Figs. 4–6, the range where the waves are observed is sensitive to the radius ratio of the cylindrical shells. It shifts to low frequencies with decreasing radius ratio.

#### 4. Radius ratio estimation of an elastic cylindrical shell

##### 4.1. Materials

The main objective of this work is to build a model that can describe the relationship between the acoustical parameters and the geometrical parameters of the cylindrical shell. We considered cylindrical shells made of copper with radius ratio between 0.50 and 0.99. As a result of the previous treatment presented in this paper, the modal isolation plan is used to determine the values of the reduced cutoff frequencies of circumferential waves. After that, the obtained reduced cutoff frequencies were implemented in a model based on artificial neural networks, with the aim to return the values of the radius ratio of the studied structure. Fig. 7 presents the reduced cutoff frequencies as a function of the radius ratio for circumferential waves, antisymmetric circumferential wave ( $A_1$ ), antisymmetric circumferential wave ( $A_3$ ), and symmetric circumferential waves ( $S_1$  and  $S_2$ ).

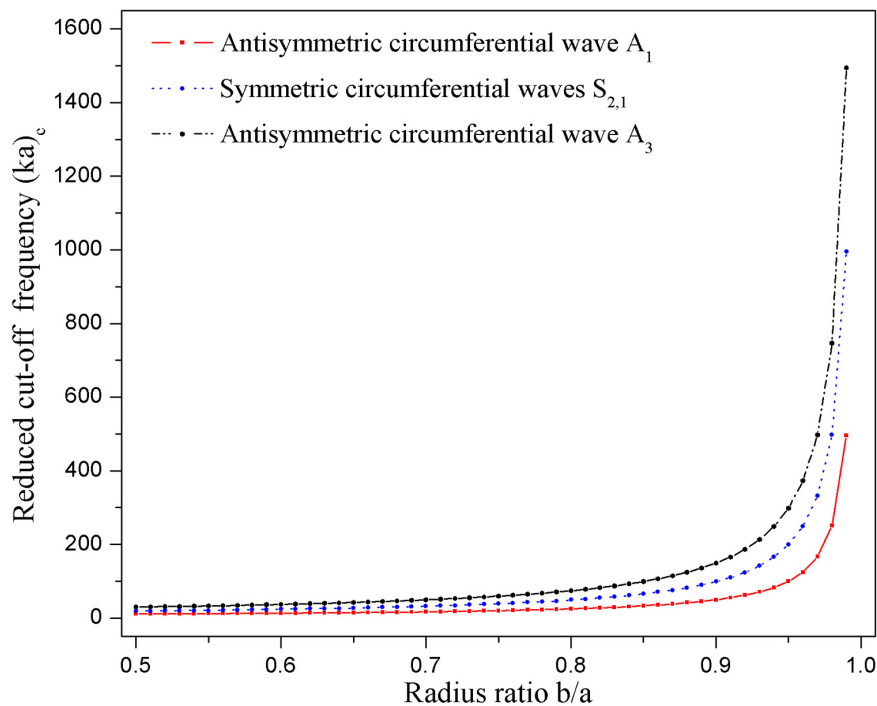


Fig. 7. Reduced cutoff frequencies of circumferential waves as a function of the radius ratio

## 4.2. Methods

### 4.2.1. Artificial neural networks

The introduction of artificial neural networks is inspired by the study of human brain [16, 30]. In practice, the neural network configuration can be divided into three parts, the input layer, hidden layer or layers, and the output layer. The input layer represents various input variables, and the output layer represents the output variables. Each layer includes integrated units called neurons. These neurons receive input variables from external sources or neurons in the previous layers, and convert them to output variables used by the neurons in the next layer. This type of networks is called feed-forward neural networks, in which the data set is processed in a feed-forward direction from the input layer to the output layer. To find the best architecture that gives the best estimation of the output data, we determine the number of hidden layers and the number of neurons in hidden layers by minimizing the error on testing data. The networks are trained by the Levenberg-Marquardt back-propagation algorithm to obtain a high generalization accuracy, which is characterized by error propagate from the last layer to the first layer in the object to adjust weights and biases of neurons in the training process. To build a reliable and robust neural network architecture, we use a strategy based on the  $k$ -fold cross-validation approach [6, 29]. The major idea of this strategy is the possibility to test and compare several configurations and combinations of input variables. Finally, the best configuration is being selected.

### 4.2.2. $k$ -fold cross-validation

Cross validation is a strategy that evaluates the performance of the model. It is used to estimate the generalization capability of the model [29]. Also, it is widely used for model selection, and becomes especially important when the data set size is considered small. There are many types of cross-validation. In this study, the  $k$ -fold cross validation was applied [6]. To implement the  $k$ -fold cross-validation, the data set is grouped randomly into  $k$  sub-samples of equal size. After that, the  $k - 1$  subsets are put together to get the training set, and the remaining subset is kept for the validation set. Then, the network training begins. This procedure is repeated  $k$  times and for each iteration the error is computed, see Fig. 8. Finally, the total performance of the model is evaluated by the average of the  $k$  performance of each iteration. The benefit of this strategy is for each example on the data set is used as the validation data once, and  $k - 1$  times as the training data.

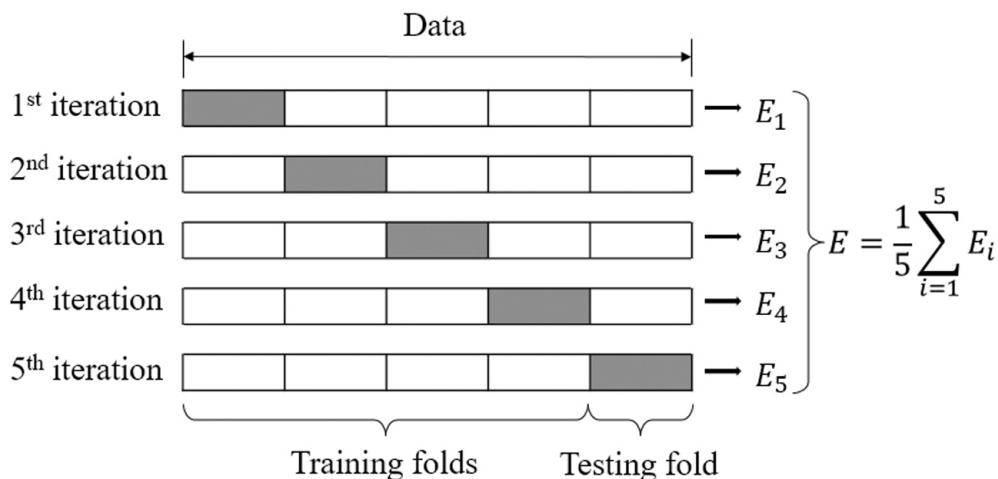


Fig. 8. Example of a 5-fold cross-validation strategy

#### 4.2.3. Evaluation of the model performance

The error criteria used in this work to investigate the performance of the proposed model is given as follows:

Mean Absolute Error (MAE)

$$\text{MAE} = \frac{1}{n} \sum_{i=1}^n |d_i - e_i|, \quad (10)$$

Mean Square Error (MSE)

$$\text{MSE} = \frac{1}{n} \sum_{i=1}^n (d_i - e_i)^2, \quad (11)$$

sample Pearson correlation coefficient ( $R$ )

$$R = \frac{\sum_{i=1}^n (d_i - \bar{d})(e_i - \bar{e})}{\sqrt{\sum_{i=1}^n (d_i - \bar{d})^2 (e_i - \bar{e})^2}}, \quad (12)$$

standard deviation ( $\sigma$ )

$$\sigma = \sqrt{\frac{1}{n} \sum_{i=1}^n (E_i - \bar{E})^2}, \quad (13)$$

where  $d$  is the target value for each variable,  $\bar{d}$  is the mean of the target values for each variable,  $e$  is the obtained value for each variable,  $\bar{e}$  is the mean of the obtained values for each variable,  $n$  is the total number of the variables in the data set,  $E_i$  is the error obtained for each iteration, and  $\bar{E}$  is the mean of all errors.

#### 4.2.4. Model development

To obtain a good neural network architecture that has an optimal number of hidden layers, optimal number of neurons in the hidden layers, and gives the best estimation of the output variables; it is necessary to build a great number of neural networks with different topologies using trial and error method. All developed network architectures have an input layer with the same input variables. The first input corresponds to the reduced cutoff frequencies of the circumferential waves, the second input corresponds to the circumferential wave type which takes the value equal to 1 for the anti-symmetric waves  $A_i$ , and equal to 0 for the symmetric waves  $S_i$ , the last input corresponds to the order of the wave, for example, 1 for  $A_1$ . All developed architectures have one output in the output layer which corresponds the value of the estimated radius ratio. For hidden layers, we tested two cases. In the first one, we tested networks with one hidden layer in which the neuron number is varied from 1 to 20. In the second one, we tested networks with two hidden layers. The number of neurons in each layer was changed from 1 to 10. In the training phase for all architectures, the  $k$ -fold cross validation strategy was applied. For each iteration, the performance was determined using the error criteria. Then, the model performance was done by calculating the average performance obtained for each iteration. In this work, the number of chosen folds  $k$  was 2, 3, 5 and 10. Finally, the optimal configuration was determined for one and two hidden layers, and for the considered number of folds  $k$ . The performance of the selected configurations was measured according to the error criteria. The diagram in Fig. 9 describes the methodology followed in this work.

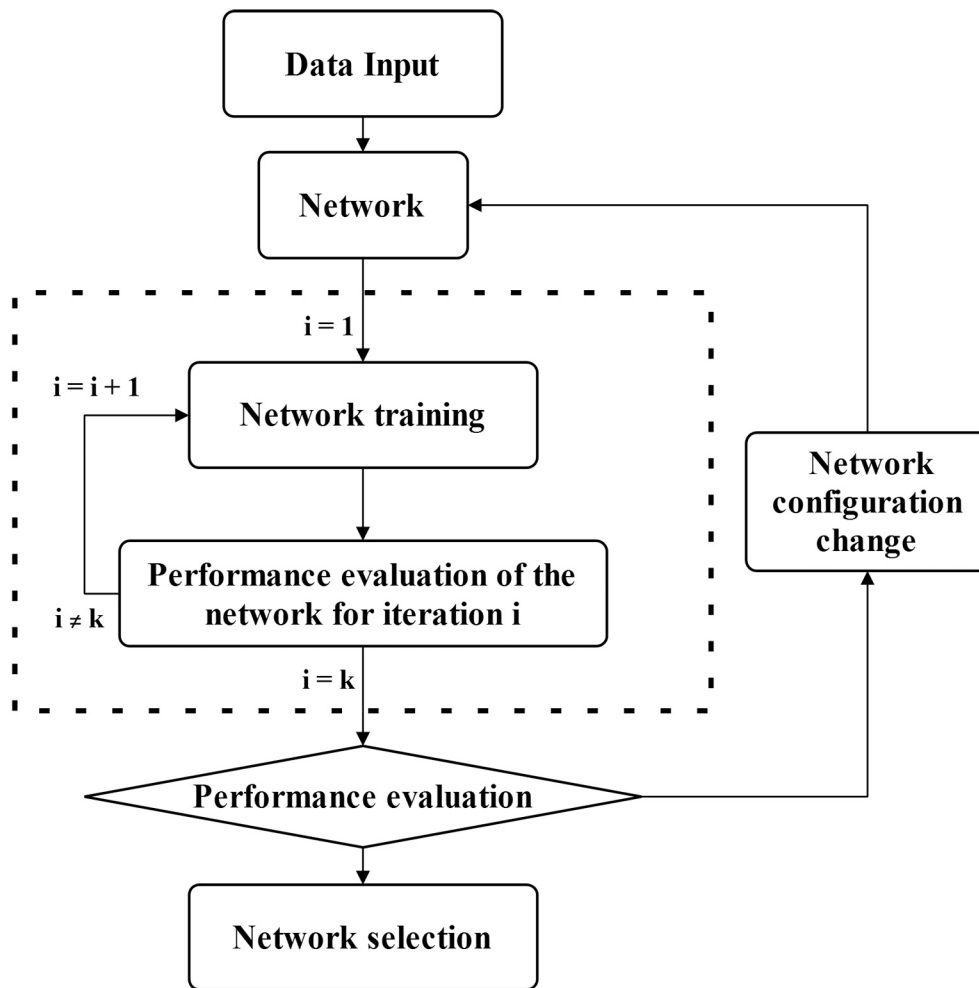


Fig. 9. Implementation methodology

## 5. Results and discussions

In this present research, the reduced cut-off frequencies of the circumferential waves ( $A_1$ ,  $A_3$ ,  $S_1$  and  $S_2$ ) are estimated using the modal isolation plan representation. These frequencies are used on a model based on the artificial neural networks to estimate the radius ratio of cylindrical shells. During the trial phase, the number of chosen folds  $k$  was 2, 3, 5 and 10, and the number of hidden layers of tested neural networks configuration was 1 and 2. Then, for every combination, we locate the successful architectures. Based on the minimum of MSE (11) and the standard deviation  $\sigma$  (13), the performance of the most successful configurations are illustrated in Table 3 and presented in Fig. 10. The arrow in Fig. 10 refers to the chosen configuration, which is a network with 2 hidden layers. Each of these two layers is made up of 5 and 6 neurons, respectively. The performance of the optimal configuration for the testing data was done according to MSE equal to  $3.1747 \times 10^{-6}$ , for the MAE equal to  $1.1787 \times 10^{-3}$ , and the sample Pearson correlation coefficient  $R = 0.99$ . These values show that there is a positive and almost perfect agreement between the desired and estimated radius ratios.

The analysis of the results obtained from the modal isolation plan shows the usefulness for estimating the reduced cutoff frequencies of circumferential waves. In this study, we considered the reduced cutoff frequencies for four waves to build a model that can return the value of the radius ratio of the cylindrical shell. This resulting model can be generalized for other waves that

Table 3. Parameters of different architectures and their performance on the testing data

	Number of folds $k$	Number of hidden layers	Number of neurons in hidden layers	MSE	$\sigma$
1	$k = 2$	1	2	$9.8813 \times 10^{-5}$	$1.3636 \times 10^{-5}$
2	$k = 3$	1	2	$3.9932 \times 10^{-4}$	$5.4081 \times 10^{-4}$
3	$k = 5$	1	2	$5.9306 \times 10^{-4}$	$4.5807 \times 10^{-4}$
4	$k = 10$	1	3	$4.5920 \times 10^{-5}$	$1.9801 \times 10^{-5}$
5	$k = 2$	2	2/6	$1.3165 \times 10^{-5}$	$4.1122 \times 10^{-6}$
6	$k = 3$	2	2/6	$5.7216 \times 10^{-5}$	$8.9668 \times 10^{-5}$
7	$k = 5$	2	5/6	$3.1747 \times 10^{-6}$	$1.3376 \times 10^{-6}$
8	$k = 10$	2	4/3	$8.8653 \times 10^{-6}$	$1.4446 \times 10^{-5}$

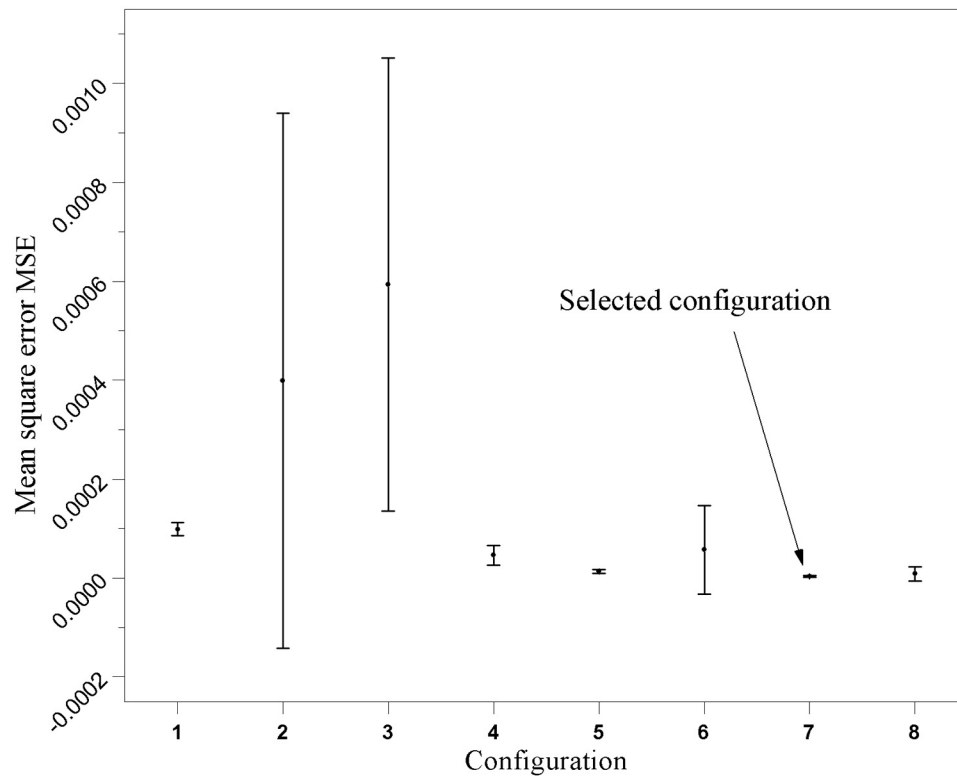


Fig. 10. Mean square error and standard deviation obtained for different configurations

are not used in this study, for this reason we applied the  $k$ -fold cross-validation strategy. The selected architecture is trained five times with different combination of the training data set in the training process, that makes our resulting model well trained. The reason for why we use four waves is that for a cylindrical shell with small values of radius ratio, the waves resonances are overlapping. Consequently, the location of the reduced cutoff frequencies of these waves becomes a little bit difficult. So, for other waves not used in this study, we just need to train the selected configuration with new data to drive a model more general than the last one.

## 6. Conclusions

The present paper is concerned with the analysis and treatments of the acoustic scattering of a plane wave from an air-filled immersed copper cylindrical shell. In this work, the model based on the artificial neural networks was developed to determine the radius ratio of the studied cylindrical shells using reduced cutoff frequencies of circumferential waves propagating around it. The first part of this paper was devoted to the estimation of the reduced cutoff frequencies of circumferential waves, which can be obtained from the resonance spectrum, the time-frequency image, or from the modal isolation plan. A comparative study was done between these methods in order to examine the quality and confronted difficulties. As a result, the reduced cutoff frequencies were estimated using the modal isolation plan. The findings showed that this representation is very useful regardless of the thickness of the cylindrical shell. The second part was devoted to the development of a model based on the artificial neural networks. During the training process, it was our aim to locate the best architecture that would give a good estimation of the radius ratio. Many networks with different configurations were developed and tested. Finally, the optimal architecture was selected. With a good accuracy, the located topology can estimate the values of the radius ratio of copper cylindrical shells. For further research, we look forward to highlight this model to estimate various parameters related to cylindrical shells made from other materials.

## References

- [1] Agounad, S., Aassif, E. H., Khandouch, Y., Elhanaoui, A., Analysis of the prediction of a bilayered cylindrical shell's reduced cutoff frequency with data-driven approaches, *Mechanical Systems and Signal Processing* 128 (2019) 126–140. <https://doi.org/10.1016/j.ymssp.2019.03.028>
- [2] Agounad, S., Aassif, E. H., Khandouch, Y., Elhanaoui, A., Signal processing techniques of circumferential waves for characterization of bilaminated cylindrical shells, *Journal of Nondestructive Evaluation* 39 (2020) 1–18. <https://doi.org/10.1007/s10921-020-0660-z>
- [3] Agounad, S., Aassif, E. H., Khandouch, Y., Maze, G., Decultot, D., Investigation into the bistatic evolution of the acoustic scattering from a cylindrical shell using time-frequency analysis, *Journal of Sound and Vibration* 412 (2018) 148–165. <https://doi.org/10.1016/j.jsv.2017.09.036>
- [4] Agounad, S., Aassif, E. H., Khandouch, Y., Maze, G., Decultot, D., Scattering of an acoustic wave by composite cylindrical shells: Influence of inner and outer layer thicknesses on the circumferential waves, *Composite Structures* 187 (2018) 439–453. <https://doi.org/10.1016/j.compstruct.2017.12.015>
- [5] Agounad, S., Aassif, E. H., Khandouch, Y., Maze, G., Decultot, D., Elhanaoui, A., Acoustic scattering from immersed composite cylindrical shells: Existence of zero group velocity circumferential waves, *Composite Structures* 182 (2017) 12–24. <https://doi.org/10.1016/j.compstruct.2017.08.093>
- [6] Arlot, S., Celisse, A., A survey of cross-validation procedures for model selection, *Statistics surveys* 4 (2010) 40–79. <https://doi.org/10.1214/09-SS054>
- [7] Chati, F., Leon, F., Maze, G., Acoustic scattering by a metallic tube with a concentric solid polymer cylinder coupled by a thin water layer. Influence of the thickness of the water layer on the two Scholte-Stoneley waves, *The Journal of the Acoustical Society of America* 118 (5) (2005) 2820–2828. <https://doi.org/10.1121/1.2065807>
- [8] Cheeke, J. D. N., Li, X., Wang, Z., Observation of flexural Lamb waves ( $A_0$  mode) on water-filled cylindrical shells, *The Journal of the Acoustical Society of America* 104 (6) (1998) 3678–3680. <https://doi.org/10.1121/1.423951>

- [9] Claasen, T. A. C. M., Mecklenbrauker, W. F. G., The Wigner Ville distribution – A tool for time-frequency signal analysis. I. Continuous-time signals, *Philips Journal of Research* 35 (3) (1980) 217–250.
- [10] Dariouchy, A., Aassif, E.H., Decultot, D., Maze, G., Acoustic characterization and prediction of the cut-off dimensionless frequency of an elastic tube by neural networks, *IEEE transactions on ultrasonics, ferroelectrics, and frequency control*, 54 (5) (2007) 1055–1064. <https://doi.org/10.1109/TUFFC.2007.351>
- [11] Elhanaoui, A., Aassif, E., Maze, G., Decultot, D., Acoustic scattering by a two-layer cylindrical tube immersed in a fluid medium: Existence of a pseudo wave, *Ultrasonics* 65 (2016) 131–136. <https://doi.org/10.1016/j.ultras.2015.10.010>
- [12] Flandrin, P., *Time-frequency*, Hermes, Paris, 1993. (in French)
- [13] Haumesser, L., *Acoustic diffusion by limited submerged cylindrical shells. Helical waves: analysis of temporal responses and complete identification of resonances*, Doctoral thesis, University of Le Havre, France, 2001. (in French)
- [14] Haumesser, L., Decultot, D., Leon, F., Maze, G., Experimental identification of finite cylindrical shell vibration modes, *The Journal of the Acoustical Society of America* 111 (5) (2002) 2034–2039. <https://doi.org/10.1121/1.1468877>
- [15] Haumesser, L., Touraine, N., Decultot, D., Maze, G., Acoustic scattering from finite cylindrical shells: Influence of end-caps (L), *The Journal of the Acoustical Society of America* 116 (4) (2004) 1901–1904. <https://doi.org/10.1121/1.1756613>
- [16] Haykin, Simon S., et al., *Neural Networks and Learning Machines*, 3 edition, Upper Saddle River: Pearson, New Jersey, 2009.
- [17] Khandouch, Y., Aassif, E. H., Agounad, S., Maze, G., A novel approach to estimate the radius ratio of an elastic tube from its form function using soft computing techniques, *International Journal of Intelligent Engineering and Systems* 9 (3) (2016) 137–145. <https://doi.org/10.22266/ijies2016.0930.14>
- [18] Laaboubi, M., Aassif, E., Latif, R., Dliou, A., Maze, G., Decultot, D., Application of the reassignment time-frequency method on an acoustic signals backscattered by an air-filled circular cylindrical shell immersed in water, *Aerospace Science and Technology* 27 (1) (2013) 216–224. <https://doi.org/10.1016/j.ast.2012.09.001>
- [19] Latif, R., Aassif, E., Laaboubi, M., Maze, G., Determination of the thickness of elastic tube using the time-frequency analysis of Wigner-Ville, *Acta Acustica united with Acustica*, 95 (5) (2009) 253–257. <https://doi.org/10.3813/AAA.918215>
- [20] Latif, R., Aassif, E., Moudou, A., Decultot, D., Faiz, B., Maze, G., Determination of the cut-off frequency of an acoustic circumferential wave using a time-frequency analysis, *NDT & E International* 33 (6) (2000) 373–376. [https://doi.org/10.1016/S0963-8695\(00\)00003-7](https://doi.org/10.1016/S0963-8695(00)00003-7)
- [21] Leon, F., *Acoustic diffusion by submerged tubes at oblique incidence, guided waves, retransmissions at the ends*, Doctoral thesis, University of Le Havre, France, 1994. (in French)
- [22] Marston, P.L., Sun, N.H., Backscattering near the coincidence frequency of a thin cylindrical shell: Surface wave properties from elastic theory and an approximate ray synthesis, *The Journal of the Acoustical Society of America* 97 (2) (1995) 777–783. <https://doi.org/10.1121/1.412124>
- [23] Maze, G., Acoustic scattering from submerged cylinders. MIIR Im/Re: Experimental and theoretical study, *The Journal of the Acoustical Society of America* 89 (6) (1991) 2559–2566. <https://doi.org/10.1121/1.400684>
- [24] Maze, G., *Diffusion of a plane acoustic wave by cylinders and tubes submerged in water: Isolation and identification of resonances*, Doctoral thesis, University of Rouen, France, 1984. (in French)
- [25] Maze, G., Izbicki, J. L., Ripoché, J., Resonances of plates and cylinders: Guided waves, *The Journal of the Acoustical Society of America* 77 (4) (1985) 1352–1357. <https://doi.org/10.1121/1.392025>

- [26] Maze, G., Leon, F., Ripoche, J., Klauson, A., Metsaveer, J., Uberall, H., Nature of the Scholte interface wave on a cylindrical shell, *Acta Acustica united with Acustica* 81 (3) (1995) 201-213. (in French) <https://doi.org/10.1051/jp4:19945184>
- [27] Morse, S. F., Marston, P. L., Meridional ray contributions to scattering by tilted cylindrical shells above the coincidence frequency: Ray theory and computations, *The Journal of the Acoustical Society of America* 106 (5) (1999) 2595–2600. <https://doi.org/10.1121/1.428091>
- [28] Pareige, P., Rembert, P., Izbicki, J. L., Maze, G., Ripoche, J., MIN numerical pulse method for isolation and identification of immersed tube resonances, *Physics Letters A* 135 (2) (1989) 143–146. (in French) [https://doi.org/10.1016/0375-9601\(89\)90662-2](https://doi.org/10.1016/0375-9601(89)90662-2)
- [29] Racine, J., Consistent cross-validatory model-selection for dependent data: *h<sub>v</sub>*-block cross-validation, *Journal of Econometrics* 99 (1) (2000) 39–61. [https://doi.org/10.1016/S0304-4076\(00\)00030-0](https://doi.org/10.1016/S0304-4076(00)00030-0)
- [30] Svozil, D., Kvasnicka, V., Pospichal, J., Introduction to multi-layer feed-forward neural networks, *Chemometrics and Intelligent Laboratory Systems* 39 (1) (1997) 43–62. [https://doi.org/10.1016/S0169-7439\(97\)00061-0](https://doi.org/10.1016/S0169-7439(97)00061-0)